In-situ Synthesis and Characterization of Ceramic Reinforced Inconel 718 Coatings Using B4C-Inconel 718 Powders by Laser Directed Laser Energy Deposition

Yunze Li
Texas Tech University
Dongzhe Zhang
Texas Tech University
Bo Zhao
Texas Tech University
Weilong Cong (weilong.cong@ttu.edu)
Texas Tech University https://orcid.org/0000-0001-6308-7383

Research Article

Keywords: Coating, Laser directed energy deposition (DED), Inconel 718 alloy, B4C, In-situ synthesis, Mechanical properties

Posted Date: January 10th, 2022

DOI: https://doi.org/10.21203/rs.3.rs-1230179/v1

Version of Record: A version of this preprint was published at The International Journal of Advanced Manufacturing Technology on March 28th, 2022. See the published version at https://doi.org/10.1007/s00170-022-09069-4.

Abstract

Inconel 718 has been widely used in aerospace, nuclear and marine industries due to excellent high-temperature mechanical properties and corrosion resistance. In recent years, laser directed energy deposition (DED) become a competitive method in the fabrication of Inconel 718 coatings. Compared with other surface coating processes, laser DED has the advantage of extremely fine-grained structures, strong metallurgical bonding, and high density. However, the hardness and wear resistance of Inconel 718 coatings still need to be improved. To further improve these properties, ceramic reinforced Inconel 718 coatings have been investigated. Compared with ex-situ ceramic reinforcements, the in-situ synthesized reinforcements have the advantage of refined ceramic particle size, uniform distribution, and low thermal stress. B_4C was a preferable additive material to fabricate in-situ synthesized multi-component ceramic reinforced Inconel 718 coatings. The addition of B_4C could form a large number of borides and carbides as ceramic reinforcements. In addition, the in-situ reactions between Inconel 718 and B_4C could release heat during the fabrication, thereby promoting the melting of material powders. However, there are currently no investigations on the in-situ synthesis mechanisms, microstructure, and mechanical properties of laser DED fabricated B_4C-Inconel 718 coatings. In this study, the effects of B_4C on the properties of Inconel 718 coatings were investigated. Results show that Ni_3B, NbB, and Cr_3C_2 phases were formed. With the addition of B_4C, the size of Laves phase was refined and the porosity was decreased. The hardness and wear resistance of B_4C reinforced coatings were improved by about 34% and 28%, respectively.

1. Introduction

Inconel 718, as a kind of nickel-based superalloy, has remarkably high-temperature mechanical properties and corrosion resistance. It is a good choice for strengthening or repairing the structural parts that are prone to be damaged under conditions with complicated stress and elevated temperature [1, 2]. In recent years, laser-directed energy deposition (DED) becomes a competitive technology for repairing and coating structural parts, due to its advantages of excellent bonding quality, easy controllability, excellent stability, and the capability of functionally gradient materials fabrication [3, 4]. Due to these advantages, the fabrication of Inconel 718 coatings on stainless steel and nickel-based alloys by laser DED process have been received extensive research attention [5, 6]. Results show that the laser DED fabricated coatings are free of micropores and micro-cracks and have good adherence to the substrates. However, the microhardness and wear resistance of laser DED fabricated Inconel 718 coatings is relatively low, which limited their further applications in many areas.

In order to improve the service life and mechanical properties of laser DED fabricated Inconel 718 coatings, ceramic materials such as BN, SiC, and Al_2O_3 have been directly added to Inconel 718 coatings as reinforcement phases [7–10]. However, the addition of ex-situ ceramic reinforcements also has a serious negative impact on the quality of coatings. Due to the high melting point of ex-situ ceramic reinforcements, the feedstock powders are hard to be fully melted. The un-melted particles could

decrease the fluidity of the molten pool, leading to the generation of fabrication defects and the uneven distribution of the ceramic reinforcements [11]. In addition, the thermal expansion coefficients of ex-situ ceramic reinforcements and Inconel 718 matrix are different. During the solidification process, the matrix cracking in composites could be generated. Different from the ex-situ process, in the in-situ process, the reinforcements are synthesized in the matrix itself by chemical reactions. The ultra-fine ceramic reinforcement particles could be generated and uniformly distributed in the fabricated coatings, which could further improve the consistency and the mechanical properties of the fabricated coatings. In addition, the large thermal expansion coefficient differences between ceramic particles and matrix are reduced, which suppresses the crack generation [12, 13].

Over the past decade, researchers have demonstrated interest in the fabrication of in-situ synthesized ceramic reinforced Inconel 718 coatings. TiC has been the most commonly used as the reactant of in-situ synthesized ceramic reinforced Inconel 718 coatings [14]. Results show that a large number of sub-grain boundaries appear in the TiC/Inconel 718 nanocomposite coatings, which significantly increases the hardness and wear resistance. Compared with TiC, B_4C has more advantages to serve as the reactant of in-situ synthesized ceramic reinforced Inconel 718 coatings. Firstly, due to the low molar mass of B_4C, a small amount of B_4C could form a large number of borides and carbides as hard phases that can significantly improve the hardness and the erosion resistance of the coating. Secondly, the borides generate from the reactions between B_4C and Inconel 718 could provide heterogeneous nucleation sites for the Laves phase during the solidification, which could refine the size of Laves phase and improve the microhardness of the fabricated coatings. Finally, the in-situ reactions between B_4C and metallic materials always generate a large amount of heat [15]. The generated heat has the potential to be utilized to promote the melting of feedstock powders and reduce the laser energy input. As far as the authors know, there are no investigations on the fabrication of in-situ synthesized ceramic reinforced Inconel 718 coatings using B_4C-Inconel 718 powders. The in-situ synthesis and characterization of the fabricated coatings are still unknown. In this study, the multi-component ceramic reinforced Inconel 718 coatings were successfully fabricated by laser DED process. The effects of B_4C on molten pool size and temperature, element and phase compositions, microstructure, porosity, and mechanical properties of the fabricated coatings (including microhardness and wear resistance) were investigated.

2. Experimental Procedures

2.1 Powder treatment

The powder materials used in this study were B_4C powder (99.7% purity) (Atlantic Equipment Engineers Inc., Upper Saddle River, NJ, USA) and Inconel 718 powders (99.7% purity) (Carpenter Powder Products Inc., Bridgeville, PA, USA). A stainless steel 304 of 6.65 mm thickness was used as the substrate. The feedstock material powders (Inconel 718 and Inconel 718 + 2 wt.% B_4C) were adopted to fabricate coatings. As shown in Figure 1, before the LDED process, B_4C powder and Inconel 718 powder were mixed by a planetary ball milling machine (ND2L, Torrey Hills Technologies LLC., San Diego, CA, USA) for

four hours with the rotation speed of 200 rpm. The weight ratio of milling balls to powders was 1:1. B_4C powders were mixed with Inconel 718 powders after the ball milling process.

2.2 Experiment setup

As shown in Figure 2, experiments were conducted on an LDED machine (LENS 450, Optomec Inc., Albuquerque, NM, USA) equipped with a 400 W fiber laser source (YLM-1070, IPG Photonics, USA). Before the fabrication, to avoid the oxidization of B4C and Ti at a high temperature, argon gas was utilized to purge the chamber system. During the fabrication, the laser beam was generated and transformed to the substrate to generate a molten pool, which caught and melted the material powders. When the laser beam moved away, the molten pool was solidified to fabricate the first layer. After the fabrication of the first layer, the cladding head moved up the distance of a layer thickness to fabricate the second layer on the top surface of the first layer. By repeating this procedure, the coatings were fabricated layer by layer. The values or ranges of input fabrication variables are listed in Table 1.

2.3 Measurement procedures

During the fabrication, An infrared thermal camera (PYROVIEW 768 N, DIAS INC, Dresden, Germany) was used to obtain the thermal images of the molten pool. The infrared thermal camera was fixed in the chamber at a 20 cm distance to the molten pool. The professional software (PYROSOFT 3.22, DIAS INC, Dresden, Germany) was used to record the collected thermal data with a sample rate of 25 Hz. The phases of the fabricated coatings were analyzed by an X-ray diffraction (XRD) machine (Ultima III, Rigaku Corp., The Woodlands, TX, USA). The samples were scanned from 20 to 80 degrees (2θ) with a scanning step of 0.02 degrees (2θ), and the parameter in XRD tests are wavelength 0.154 nm, voltage 40 kV, and current 44 mA. Each peak was fitted by the MDI/JADE software (Version 2020, Materials Data, Livermore, CA, USA). A scanning electron microscope (SEM) (Crossbeam 540, Carl Zeiss AG, Oberkochen, Germany) was used to observe the microstructure morphologies of the fabricated coatings. An energy dispersive X-ray spectroscopy (EDS) system equipped was used to analyze the element compositions. Before the observation, a thin Iridium layer was coated on the samples to create excellent conductivity and the signal to noise ratio dramatically, resulting in crisp and clear SEM images. To further quantify the size and volume content of the reinforcements, the Image J software was utilized to process the SEM images for both Inconel 718 coatings and B_4C-Inconel 718 coatings under the mode of black and white. The volume fraction of Laves phase is quantified by the area ratio of Laves phase in the cross-sectional surface. To obtain an accurate result, for both Inconel 718 coatings and B_4C-Inconel 718 coatings, five cross-sectional surfaces were analyzed to get the average volume fractions of Laves phases.

The microhardness of the deposited coating layers was tested by a Vickers microhardness tester (Phase II, Upper Saddle River, NJ, USA) with a 10 N normal load. Two samples fabricated by the LDED process were tested to measure the microhardness. For each sample, the microhardness test was performed ten times on random positions of the polished surface. The wear rate was tested and measured by dry sliding tests with a silicon carbide ball at room temperature using a mechanical testing system (PB1000,

Nanovea, Manufacturer in Irvine, CA, USA). During the dry sliding test, the SiC ball was sliding on the surface of the coating for 15 minutes with a load of 0.2 N, a constant sliding speed of 3mm/s, and a sliding distance of 3 mm. An OLYMPUS DSX-510 optical microscope (OM) (Tokyo, Japan) was used to observe the worn surface and obtain the scratching width after the dry sliding tests. The wear rate W_r was calculated by Eq.1.

$$W_r = \frac{V}{F(vT)} \quad (1)$$

where, V was the wear volume lost, mm^3, F was the normal load, N; v was the sliding speed, mm/s; T was the duration time, s.

3. Results And Discussion

3.1 Phase composition

Figure 3 shows the XRD results of the phase composition analysis on Inconel 718 coatings and B_4C-Inconel 718 coatings. In the XRD results of Inconel 718 coatings, the peaks matched up reasonably well for a γ Ni-Cr-Fe phase (PDF-# 65-0380) but were shifted to the left slightly. Most likely there were a small amount of other Nb-rich and Mo-rich precipitations doped into the structure. Similar results were also reported in the laser DED fabricated Inconel 718 parts [16,17]. With the addition of B_4C, some new phases include Ni_3B (PDF-# 48-1223), NbB (PDF-# 32-0709), and Cr_2C_3 (PDF-# 65-0897) were identified by the XRD analysis. In addition, there was no peak representing B_4C in the XRD results. It could be confirmed that the feedstock B_4C powders were completely reacted with Inconel 718 to form multi-component ceramic reinforcements during the fabrication. Inconel 718 as a kind of nickel-chromium alloy also contained significant amounts of niobium, iron, and molybdenum along with lesser amounts of aluminum and titanium. Because of the instability of B_4C in liquid metallic materials, there were in-situ reactions to form Ni_3B, NbB, and Cr_3C_2 phases:

$$12Ni + 4Nb + 3Cr + 2B_4C \rightarrow 4Ni_3B + 4NbB + Cr_3C_2 \quad (2)$$

It could also be seen that compared with Inconel 718 coatings, the intensity of the Ni-Cr-Fe peaks in B_4C-Inconel 718 coatings was slightly decreased. The major reason was that Ni and Cr reacted with B_4C to form ceramics during the fabrication, reducing the content of Ni-Cr-Fe. The positions of Ni-Cr-Fe peaks in B_4C-Inconel 718 coatings were further shifted to the left, which was farther to the positions of the standard Ni-Cr-Fe phase. The peak shift indicated that the content of Nb-rich and Mo-rich precipitations (Laves phase) in B_4C-Inconel 718 coatings was higher than that in Inconel 718 coatings.

3.2 Molten pool size and temperature

The thermal image of the molten pool for the 3 layers single track coatings (t = 25s) and the maximum temperature during the fabrication are shown in Figure 4. As shown in Figure 4(a), the shape of both Inconel 718 coatings and B_4C-Inconel 718 coatings was an irregular circle, when taking the melting point of the Inconel 718 (1450 °C) as the molten pool boundaries. With the same laser deposition input parameters of laser power, hatch distance, scanning speed, and powder feed rate, the molten pool size of B_4C-Inconel 718 coatings (~ 2.25 mm) was much larger than that of Inconel 718 coatings(~ 1.35 mm). As shown in Figure 4(b), the maximum temperature of Inconel 718 coatings was slightly increased from 1700 °C to 1800 °C during the fabrication due to the heat accumulation effects. As a comparison, the maximum temperature of B_4C-Inconel 718 coatings was much higher than Inconel 718 coatings, which were significantly increased from 1900 °C to 2200 °C during the fabrication. The higher temperature increasing rate and the higher maximum temperature of B_4C-Inconel 718 coatings indicated that the in-situ reactions between B_4C and Inconel 718 released a large amount of heat [15]. A larger molten pool size and higher molten pool temperature had the potential to increase the fluidity of the liquid materials in the molten pool, which could improve the bonding quality, coating density, and reinforcement distribution.

3.3 Element composition and microstructure

3.3.1 Analysis of element composition

Figure 5 shows the element compositions of Inconel 718 coatings and B4C-Inconel 718 coatings. In Inconel 718 coatings, there were white regions distributed in a grey matrix. Point 1 and point 2 were probed in the white regions and grey matrix regions, respectively. The element compositions of the white regions and grey matrix regions were shown in Table 2(a). Both white regions and grey matrix regions were rich in Ni, Cr, and Fe. Compared with grey matrix regions, white regions had a higher content of Nb and Mo and represented the Laves phase, which was generated during the solidification process through the segregation of Nb and Mo from the matrix [18,19]. The grey matrix regions were Ni-Cr-Fe phase, in which the contents of Nb and Mo were lower than that in feedstock Inconel 718 powders. The reason was that the formation of Laves phase consumed the solid solution elements of Nb and Mo in the matrix.

Different from the Inconel 718 coatings, there were three kinds of regions in B_4C-Inconel 718 coatings. Besides the white precipitated regions and the grey matrix regions, there were also irregular black regions distributed near the white regions. The size and morphology of black regions were different from the feedstock B_4C powders, which could be considered as the in-situ synthesized ceramic reinforcement. As discussed in Section 3.1, during the fabrication, there were in-situ reactions between B_4C and Inconel 718 to form Ni_3B, NbB, and Cr_3C_2. To further investigate the composition of the in-situ synthesized ceramic reinforcement, point 1 and point 2 were probed in the black regions and grey matrix, respectively. The detailed element compositions of different regions were shown in Table 2(b). In the black regions, the major elements were Ni, B, Cr, and C. Compared with the grey matrix regions, the black regions had higher element content of B and C, indicating the black regions were mainly borides and carbides that were

formed through the reactions between B_4C and Inconel 718. Combined with the XRD results, the black regions could be confirmed as the in-situ synthesized ceramic reinforcements of Ni_3B, NbB, and Cr_2C_3.

3.3.2 Analysis of microstructural morphology

Figure 6(a) shows the comparisons on microstructural morphologies of Inconel 718 coatings and B_4C-Inconel 718 coatings fabricated by laser DED process. In Inconel 718 coatings, it could be seen that the growth of long strip-shaped precipitated Laves phase was in the building direction (vertical direction). This phenomenon was caused by the unidirectional solidification direction. During the fabrication of Inconel 718 coatings and B_4C-Inconel 718 coatings by the laser DED process, the localized heat flux within the molten pool was the main factor influencing the grain growth, which was usually vertical downward due to the good thermal conductivity of Ti substrates [2]. The gradient of temperature in the vertical direction was higher than that in the horizontal direction, leading to the bottom-up generation of Laves phase.

With the addition of B_4C, the in-situ formed ceramic reinforcements were generated along with the precipitated Laves phase. The ceramic reinforcements and Laves phase were uniformly distributed in laser DED fabricated B_4C-Inconel 718 coatings. The formation mechanism could be in three stages:

Firstly, the laser beam melted the substrates and generated a molten pool. As discussed in Section 3.1, the temperature of the molten pool reached the melting point of B_4C during the fabrication. Both B_4C and Inconel 718 powders were fully melted to form the liquid-state mixture. The added B element would react with part of liquid Nb and Ni constituent to form liquid NbB and Ni_3B.

Secondly, when the laser beam moved away, the liquid materials in the molten pool cooled down and started to be solidified. In the beginning, due to the high melting point, NbB and Ni_3B precipitated and grew into long strip particles, which provided nucleation sites for the Laves phase. Then, the Laves phase nucleated around the ceramics in the liquid Ni-Cr-Fe.

Finally, the liquid Ni-Cr-Fe solidified to generate the matrix. The in-situ formed ceramics and precipitated Laves phase were uniformly distributed in the Ni-Cr-Fe matrix.

To further investigate the morphology, size, and volume fraction of precipitated Laves phase, the SEM images under the mode of black (matrix and ceramic reinforcement) and white (precipitated Laves phase) were shown in Figure 6 (b). With the addition of B_4C, the size of precipitated Laves phase in B_4C-Inconel 718 coatings was decreased. The major reason was that the element B from the decomposition of B_4C reacted with Inconel 718 and then formed boride particles, which could act as the active nuclei in the molten pool. A large number of active nuclei increased the number of precipitated Laves phase grains in a certain melting volume, which suppressed the growth of Laves phase into a coarse strip-shaped structure during the solidification. It could be also seen that with the addition of B_4C, the volume fraction of Laves phase was significantly decreased from 17.742% to 6.396%. The major reason was that

the Nb, an important constituent element of the laves phase, reacted with B_4C to form NbB during the fabrication, resulting in the lower Nb content in the molten pool. As a result, the formation of Laves phase in B_4C-Inconel 718 coatings was suppressed. Similar results had been reported in the Inconel 625 with 0.4 wt.% boron coatings fabricated by the gas tungsten arc deposition process [20].

3.4 Fabrication Defects

The effects of B_4C on the fabrication defects of Inconel 718 coatings were shown in Figure 7. It can be seen that the irregular-shaped defects were distributed in the In Inconel 718 coatings. As a comparison, there was no irregular-shaped defect in the B_4C-Inconel 718 coatings. In the LDED process, the irregular-shaped fabrication defects on the cross sectional surface were usually caused by the lack of fusion, as demonstrated by Zhang et al. [21]. Since the molten pool size and temperature of B_4C-Inconel 718 coatings were much larger than that of Inconel 718 coatings (as discussed in Section 3.1), more feedstock powders could be caught and fully melted by the molten pool. The formation of sufficient overlaps was promoted, which could reduce the lack of fusion at the boundaries of the molten pool.

It can be also seen that there were also some micropores distributed in both Inconel 718 coatings and B_4C-Inconel 718 coatings. In the laser DED process, the cooling rate was extremely high. Entrapped gas bubbles were difficult to be efficiently expelled before the molten pool solidified [22]. Compared with Inconel 718 coatings, the number of micropores in B_4C-Inconel 718 coatings was much smaller than that in Inconel 718 coatings. There were two major reasons. Firstly, due to the heat generated from the in-situ reactions between B_4C and Inconel 718, the molten pool of B_4C-Inconel 718 coatings had the thermodynamic conditions with higher fluidity. Gas bubbles could float upward faster and escape from the molten pool before the molten pool solidification. Secondly, the solidification process of B_4C-Inconel 718 coatings during the fabrication was extended by the exothermic reactions and the melting point depressant (B element), which could also promote the escape of gas bubbles[20].

3.5 Analysis of mechanical properties

3.5.1 Microhardness

Figure 8 shows the comparison of the microhardness of Inconel 718 coatings and B_4C-Inconel 718 coatings fabricated by laser DED process. The microhardness of B_4C-Inconel 718 coatings (348 HV) was significantly higher than that of Inconel 718 coatings (264 HV). As discussed in Section 3.3, ceramic reinforcement particles were uniformly distributed in the Ni-Cr-Fe matrix. These reinforcements had higher hardness than Inconel 718 alloy, which could bear the load during the microhardness tests. In addition, it was well known that a large amount of Laves phase in the form of long-strip morphology was detrimental to the strength and hardness of Inconel 718 since it depletes the elements needed for precipitation strengthening. With the addition of B_4C, the coarse and long strip-shaped Laves phase was changed to needle-shaped Laves phase with refined size, uniformed distribution, and lower volume fraction. The negative impacts of Laves phase on mechanical properties of Inconel 718 coatings were

greatly reduced. In addition, the microhardness was positively correlated to the density. As discussed in Section 3.4, with the addition of B_4C, the fabrication defects and micropores were significantly decreased, which increased the ability to support the load and improve the microhardness.

3.5.2 Wear resistance

Figure 9 shows the differences in the morphology of worn surfaces between the Inconel 718 coatings and B_4C-Inconel 718 coatings. In the dry sliding tests of Inconel 718 coatings, scratches and a large area of coating delamination can be observed on the worn surface of the Inconel 718 laser cladding layer. These features indicated that local cold welds between the coating surfaces and silicon balls occurred under a load. Such phenomenon always occurred in adhesive wear, which had been reported by Hurricks et al. [23]. In addition, some grooves could also be observed on the worn surface of Inconel 718 coatings, which occurred when a hard surface (SiC ball) pass over a soft surface (Inconel 718 coatings). The wear mechanism of Inconel 718 coatings in the dry sliding tests was the combination of adhesive wear and abrasive wear. Compared with Inconel 718 coatings, the worn surface of laser DED fabricated B_4C-Inconel 718 coatings showed less delamination and smoother grooves. The major reason was that the high hardness of the B_4C-Inconel 718 coatings made it difficult for the silicon ball to penetrate into the surface. The morphologies of the worn surfaces indicated that the abrasive wear played a dominant role in the B_4C-Inconel 718 coatings.

Figure 10 shows the wear rate of Inconel 718 coatings and B_4C-Inconel 718 coatings. The wear rate of B_4C-Inconel 718 coatings was much smaller than that of Inconel 718 coatings, indicating a higher wear resistance. As discussed in Section 3.5.1, the microhardness of B_4C-Inconel 718 coatings was much higher than that of Inconel 718 coatings. According to Archard's wear equation, the volume of wear is inversely proportional to the hardness of the material. The higher hardness of B_4C-Inconel 718 coatings also had a great influence on the improvement of wear resistance. In addition, the metal matrix composite coatings with higher density always showed excellent wear resistance. Compared with Inconel 718 coatings, there were fewer fabrication defects in B_4C-Inconel 718 coatings, which was attributed to suppressing fracture and the spalling of hard particles and hard protuberances during the dry sliding test. Besides the effects of hardness and density on wear resistance, the wear mechanism also had great impacts on the wear resistance. The B_4C-Inconel 718 coatings with abrasive wear type had a smoother worn surface, which could reduce the coefficient of friction during the dry sliding test. Under the same test condition, the friction force was reduced, resulting in a smaller material removal volume and higher wear resistance.

4. Conclusions

In this study, the in-situ synthesized semicontinuous network microstructural ceramic reinforced Inconel 718 coatings were fabricated by laser DED process. The in-situ synthesis of the fabricated B_4C-Inconel

718 coatings and the effects of B_4C on the phase composition, microstructure, microhardness, and wear resistance were investigated. The major conclusions are drawn as follows:

1. During the laser DED process, there were reactions between B_4C and Inconel 718 to form Ni_3B, NbB, and Cr_2C_3. During the solidification, the needle-shaped NbB and Ni_3B whiskers were uniformly distributed in Inconel 718 matrix and provided nucleation sites for the Laves phase. With the addition of B_4C, the size and volume fraction of Laves phase were significantly reduced.

2. The in-situ reactions generated a large amount of heat. The molten pool temperature was significantly increased, which could suppress the formation of the lack of fusion defects and micropores in B_4C-Inconel 718 coatings.

3. With the addition of B_4C, the microhardness of B_4C-Inconel 718 coatings was significantly increased due to the generation of ceramic reinforcements and the refinement of Laves phase. The wear mechanism of B_4C-Inconel 718 coatings was abrasive wear, which was different from the Inconel 718 coatings (adhesive and abrasive wear). The wear resistance of B_4C-Inconel 718 coatings was higher than Inconel 718 coatings because of higher hardness, lower porosity, and smoother worn surface.

Declarations

Acknowledgments Not applicable

Funding The test of Raman spectroscopy in this study was supported by NSF CAREER Grant No. DMR-1760668.

Conflict of interest The authors declare no competing interests.

Availability of data and material The data supporting the conclusions are included in the article.

Code availability Not applicable.

Authors' contributions Yunze Li: methodology, investigation, validation, writing—original draft. Dongzhe Zhang: investigation, writing—review and editing. Bo Zhao: investigation. Weilong Cong: writing—review and editing.

Ethics approval The authors confirm that they have abided by the publication ethics and state that this work is original and has not been used for publication anywhere before.

Consent to participate The authors are willing to participate in journal promotions and updates.

Consent for publication The authors give consent to the journal regarding the publication of this work.

References

[1] Ning, F., Hu, Y., Liu, Z., Cong, W., Li, Y., & Wang, X. (2017). Ultrasonic vibration-assisted laser engineered net shaping of Inconel 718 parts: a feasibility study. *Procedia Manufacturing, 10*, 771-778.

[2] Wang, H., Hu, Y., Ning, F., & Cong, W. (2020). Ultrasonic vibration-assisted laser engineered net shaping of Inconel 718 parts: Effects of ultrasonic frequency on microstructural and mechanical properties. *Ceramics International, 276*, 116395.

[3] Hu, Y., & Cong, W. (2018). A review on laser deposition-additive manufacturing of ceramics and ceramic reinforced metal matrix composites. *Ceramics International, 44*(17), 20599-20612.

[4] Wang, L., Felicelli, S., Gooroochurn, Y., Wang, P., & Horstemeyer, M. (2008). Optimization of the LENS® process for steady molten pool size. *Materials Science Engineering: A, 474*(1-2), 148-156.

[5] Tabernero, I., Lamikiz, A., Martínez, S., Ukar, E., & Figueras, J. (2011). Evaluation of the mechanical properties of Inconel 718 components built by laser cladding. *International Journal of Machine Tools Manufacture, 51*(6), 465-470.

[6] Lambarri, J., Leunda, J., Navas, V. G., Soriano, C., & Sanz, C. (2013). Microstructural and tensile characterization of Inconel 718 laser coatings for aeronautic components. *Optics Lasers in Engineering, 51*(7), 813-821.

[7] Kim, S. H., Shin, G.-H., Kim, B.-K., Kim, K. T., Yang, D.-Y., Aranas, C., . . . Yu, J.-H. (2017). Thermo-mechanical improvement of Inconel 718 using ex situ boron nitride-reinforced composites processed by laser powder bed fusion. *Scientific reports, 7*(1), 1-13.

[8] Zemzemi, F., Rech, J., Salem, W. B., Dogui, A., & Kapsa, P. (2014). Identification of friction and heat partition model at the tool-chip-workpiece interfaces in dry cutting of an Inconel 718 alloy with CBN and coated carbide tools. *Advances in Manufacturing Science Technology, 38*(1).

[9] Sahu, S. K., Jadam, T., Datta, S., & Nandi, G. (2018). Effect of using SiC powder-added dielectric media during electro-discharge machining of Inconel 718 superalloys. *Journal of the Brazilian Society of Mechanical Sciences Engineering, 40*(7), 1-19.

[10] Yu, Z., Tan, H., Wang, S., Cheng, J., Sun, Q., Yang, J., & Liu, W. (2020). High-temperature tribological behaviors of MoAlB ceramics sliding against Al_2O_3 and Inconel 718 alloy. *Ceramics International, 46*(10), 14713-14720.

[11] Zhang, D., Li, Y., Wang, H., & Cong, W. (2021). An investigation on Ni4Ti3 phase precipitation and its effects in laser directed energy deposition of TiC–NiTi composites. *Materials Science Engineering: A,809*, 140976.

[12] Zhang, X., Song, F., Wei, Z., Yang, W., & Dai, Z. (2017). Microstructural and mechanical characterization of in-situ TiC/Ti titanium matrix composites fabricated by graphene/Ti sintering

reaction. *Materials Science Engineering: A, 705*, 153-159.

[13] Xia, M., Liu, A., Hou, Z., Li, N., Chen, Z., & Ding, H. (2017). Microstructure growth behavior and its evolution mechanism during laser additive manufacture of in-situ reinforced (TiB+ TiC)/Ti composite. *Journal of Alloys Compounds, 728*, 436-444.

[14] Muvvala, G., Karmakar, D. P., & Nath, A. K. (2018). In-process detection of microstructural changes in laser cladding of in-situ Inconel 718/TiC metal matrix composite coating. *Journal of Alloys Compounds, 740*, 545-558.

[15] Zhao, Y., Yu, T., Sun, J., & Jiang, S. (2020). Microstructure and properties of laser cladded B_4C/TiC/Ni-based composite coating. *International Journal of Refractory Metals Hard Materials,86*, 105112.

[16] Liu, Y., Li, X., Li, Y., Zhao, Z., & Bai, F. (2016). The lattice distortion of nickel particles generated by spark discharge in hydrocarbon dielectric mediums. *Applied Physics A, 122*(3), 174.

[17] Kaynak, Y., & Tascioglu, E. (2018). Finish machining-induced surface roughness, microhardness and XRD analysis of selective laser melted Inconel 718 alloy. *Procedia Cirp, 71*, 500-504.

[18] Radhakrishna, C., & Rao, K. P. (1997). The formation and control of Laves phase in superalloy 718 welds. *Journal of Materials Science, 32*(8), 1977-1984.

[19] Janaki Ram, G., Venugopal Reddy, A., Prasad Rao, K., & Madhusudhan Reddy, G. (2004). Control of Laves phase in Inconel 718 GTA welds with current pulsing. *Science technology of welding joining, 9*(5), 390-398.

[20] Tian, Y., Ouyang, B., Gontcharov, A., Gauvin, R., Lowden, P., & Brochu, M. (2017). Microstructure evolution of Inconel 625 with 0.4 wt% boron modification during gas tungsten arc deposition. *Journal of Alloys Compounds, 694*, 429-438.

[21] Zhang, B., Li, Y., & Bai, Q. (2017). Defect formation mechanisms in selective laser melting: a review. *Chinese Journal of Mechanical Engineering, 30*(3), 515-527.

[22] Li, Y., Zhang, D., Wang, H., & Cong, W. (2021). Fabrication of a TiC-Ti Matrix Composite Coating Using Ultrasonic Vibration-Assisted Laser Directed Energy Deposition: The Effects of Ultrasonic Vibration and TiC Content. *Metals, 11*(5), 693.

[23] Hurricks, P. (1973). Some metallurgical factors controlling the adhesive and abrasive wear resistance of steels. A review. *Wear, 26*(3), 285-304.

Tables

Table 1. Laser coating parameters of B_4C-Inconel 718 coatings

Input fabrication variables	Values
Laser power (W)	225
Beam diameter of laser (μm)	400
Wavelength of laser (nm)	1064
Deposit head scanning speed (mm/min)	508
Hatch distance (μm)	340
Layer thickness (μm)	432
Powder feeding rate (g/min)	2
Number of layers	3
Argon gas flow rate (L/min)	6
Scanning orientation (º)	0, 90, 180, 270

Table 2(a). Element composition of Inconel 718

Element	P1 Atomic percent (%)	P2Atomic percent (%)
Ni	47.31	45.95
Cr	20.46	24.84
Fe	15.56	21.50
Nb	9.95	3.47
Mo	5.16	3.34
Ti	1.35	0.67
Al	0.21	0.23

Table 2(b). Element composition of B_4C-Inconel 718

Element	P1 Atomic percent (%)	P2 Atomic percent (%)
Ni	29.63	51.40
B	29.28	—
Cr	17.36	18.04
C	7.11	7.30
Fe	6.55	19.55
Nb	5.66	1.45
Mo	2.91	1.40
Ti	1.30	0.32
Al	0.20	0.54

Figures

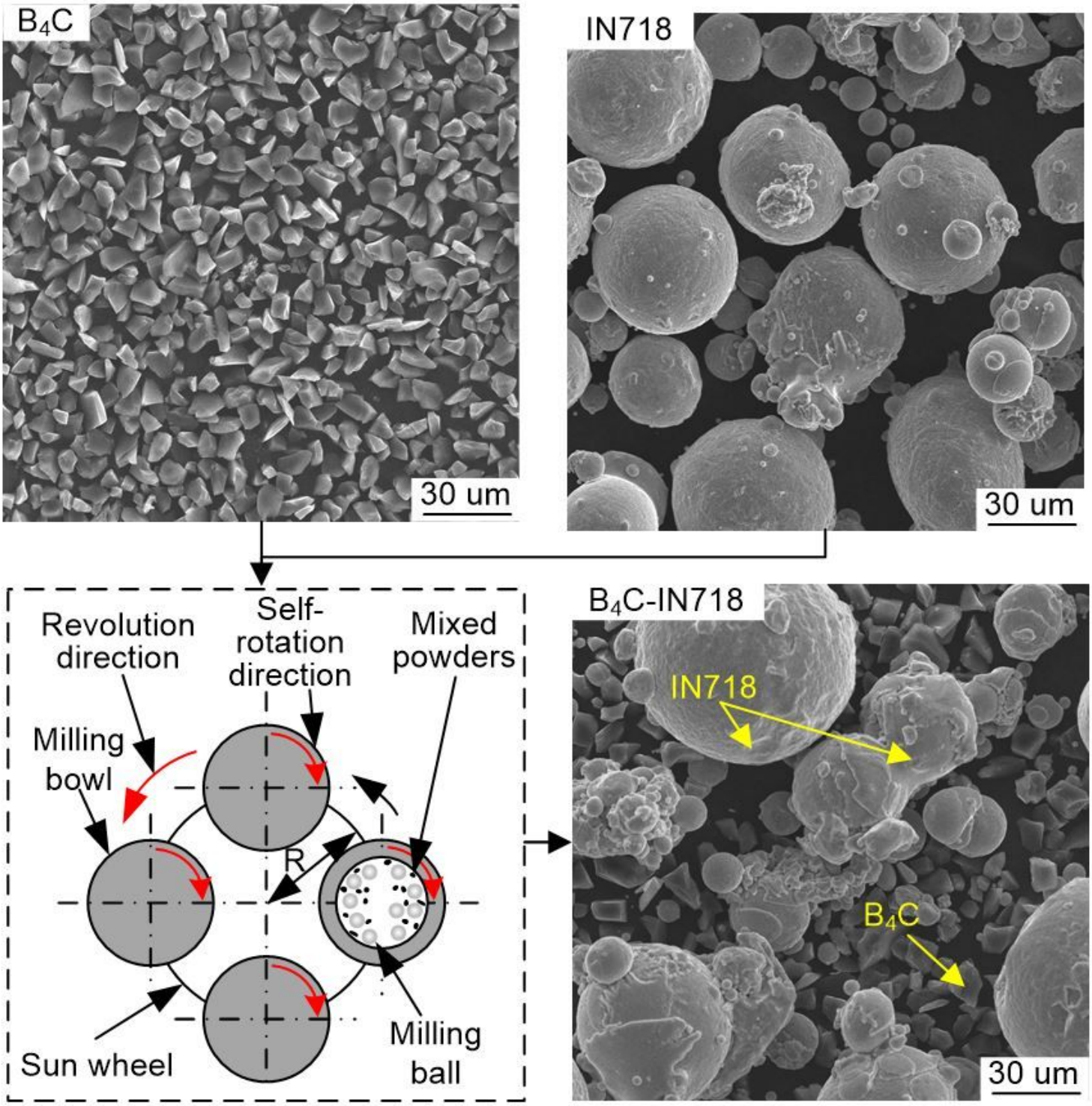

Figure 1

Powder treatment

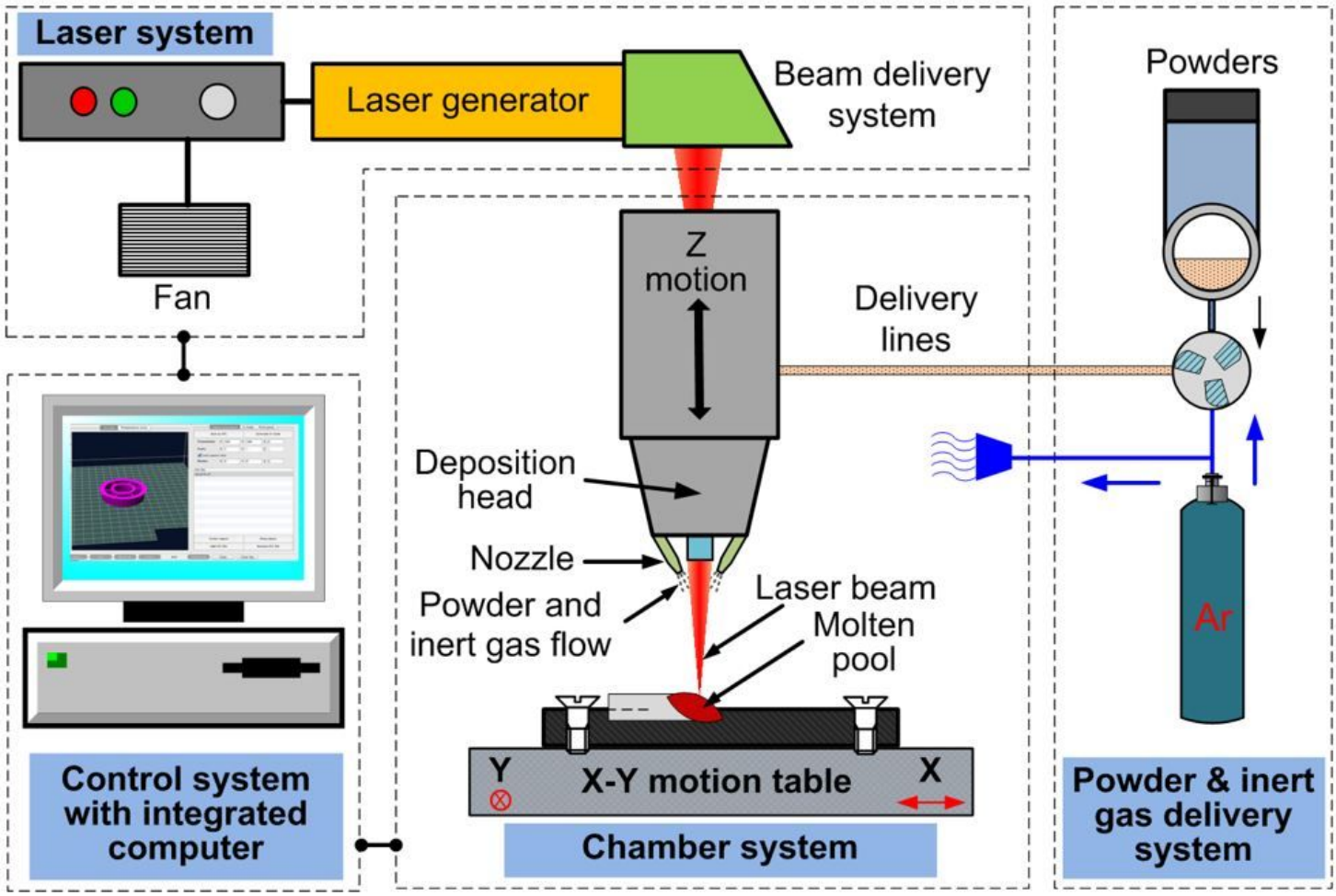

Figure 2

Experimental setup

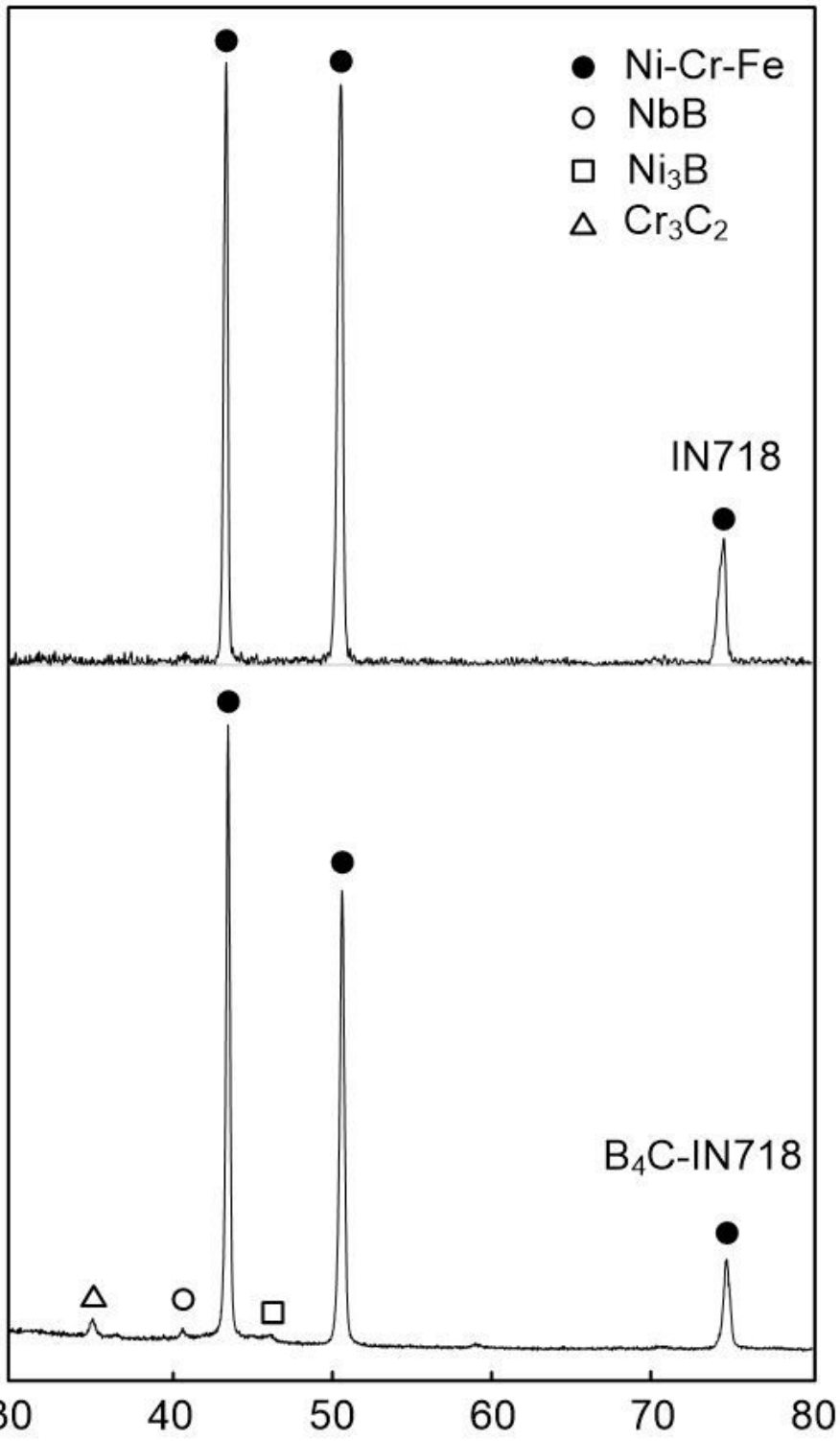

Figure 3

The phase composition of laser DED fabricated Inconel 718 coatings and B_4C-Inconel 718 coatings.

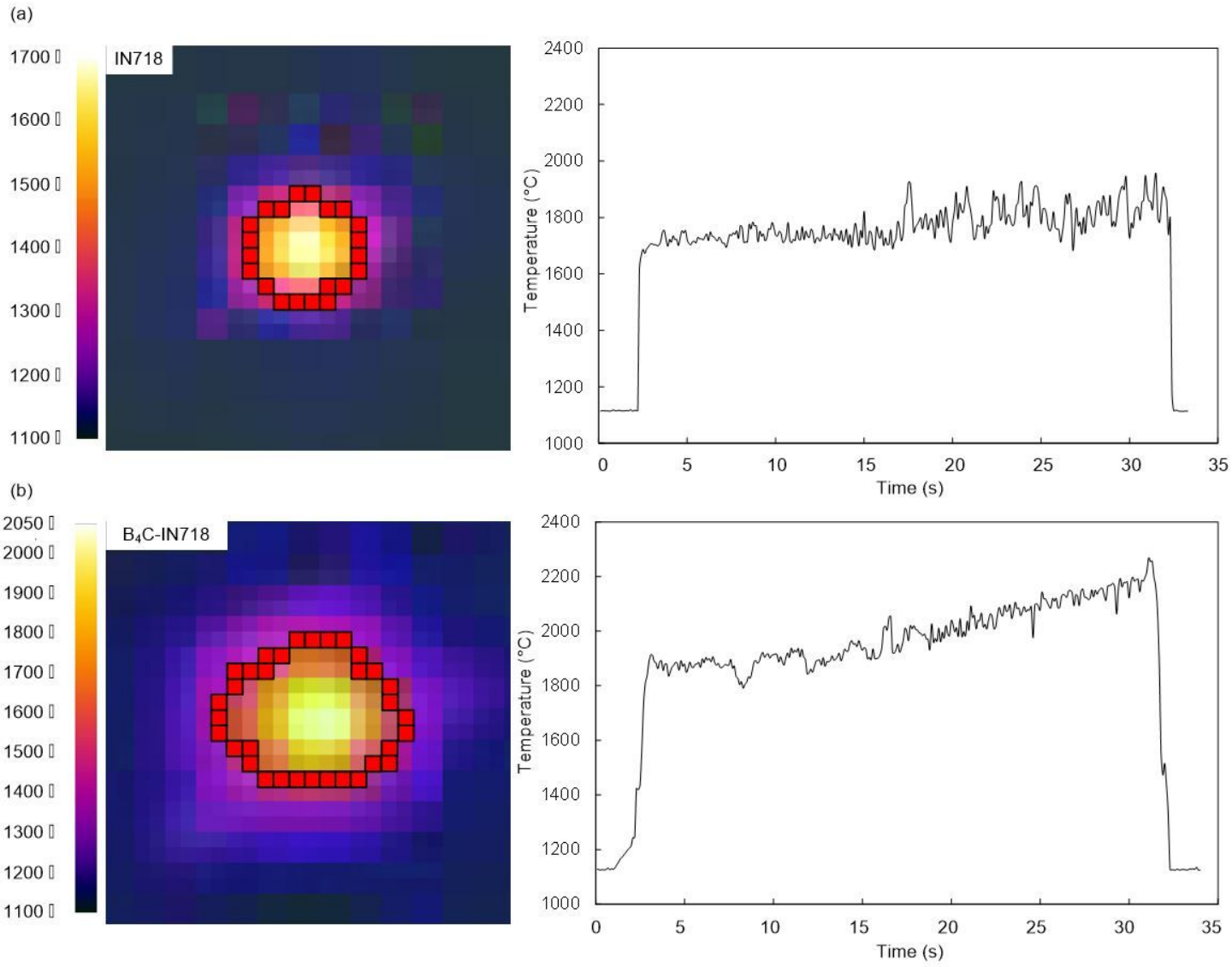

Figure 4

Molten pool size and maximum temperature: (a) Inconel 718 and (b) B_4C-Inconel 718

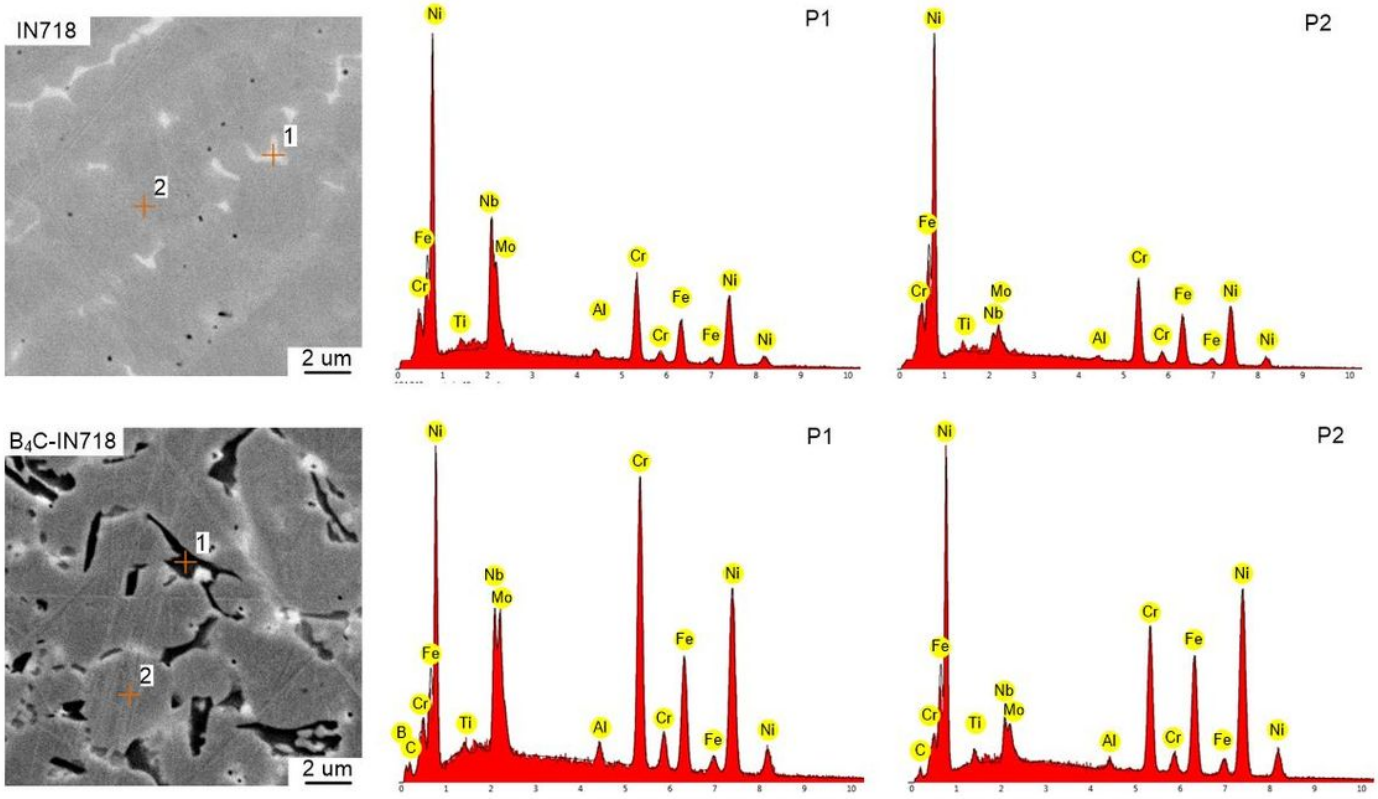

Figure 5

Element composition of laser DED fabricated Inconel 718 coatings and B_4C-Inconel 718 coatings

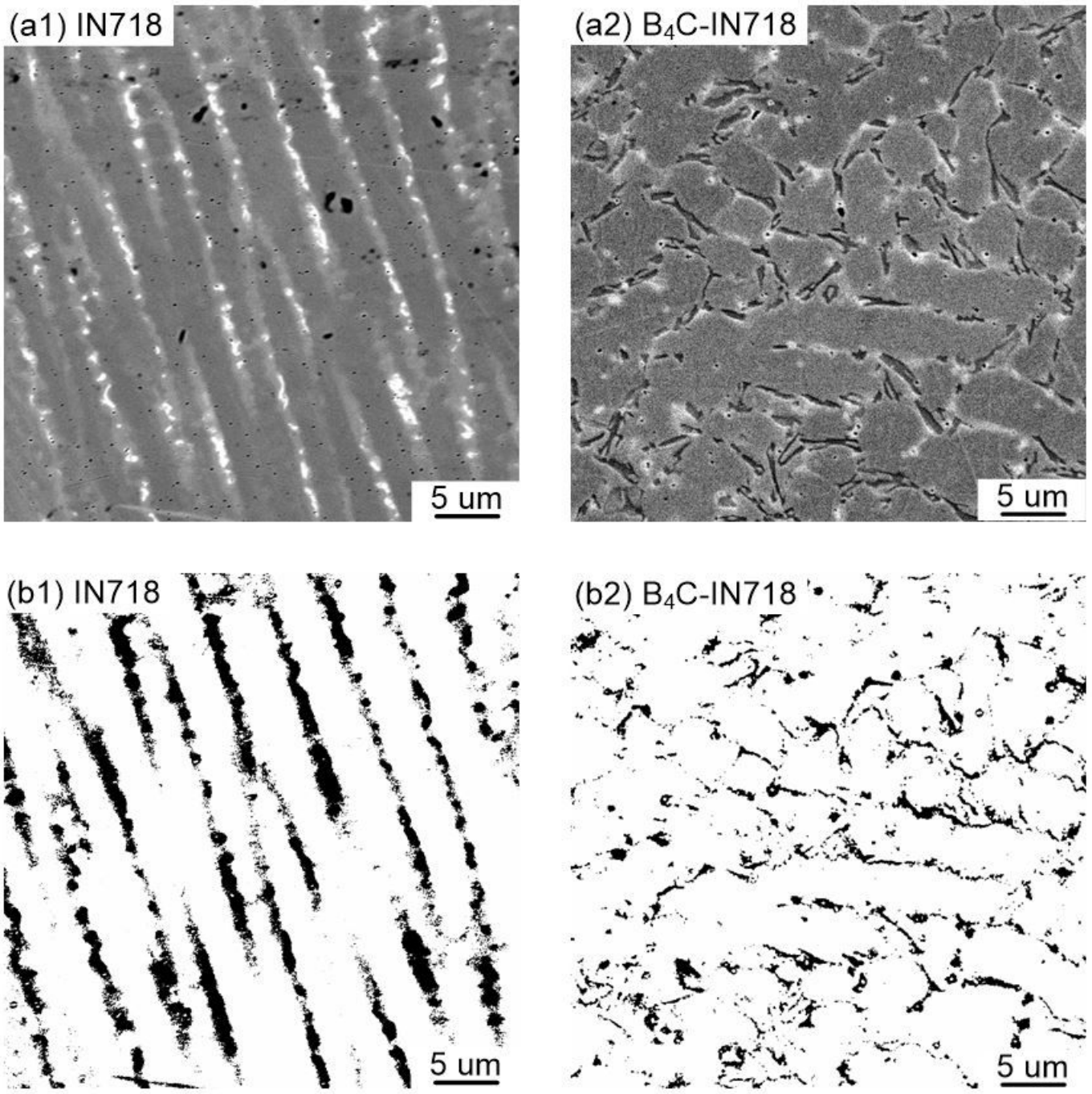

Inconel 718	B4C-Inconel 718
17.742% Laves phase	6.396% Laves phase

Figure 6

Microstructure of laser DED fabricated Inconel 718 coatings and B_4C-Inconel 718 coatings. * The Laves phase was shown as the black regions in (b1) Inconel 718 and (b2) B4C-Inconel 718

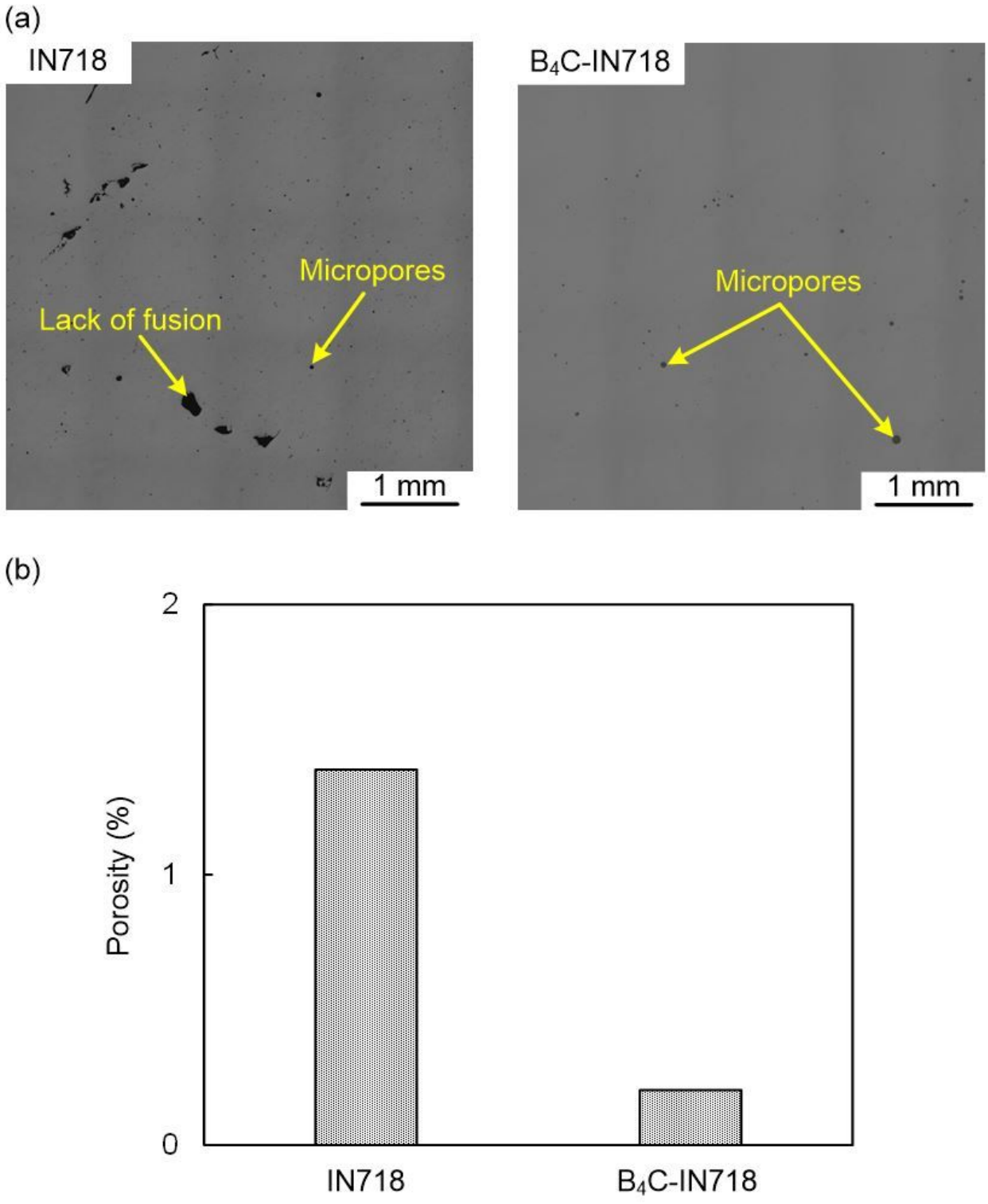

Figure 7

Porosity of laser DED fabricated Inconel 718 coatings and B_4C-Inconel 718 coatings: (a) optical microscope image and (b) porosity values

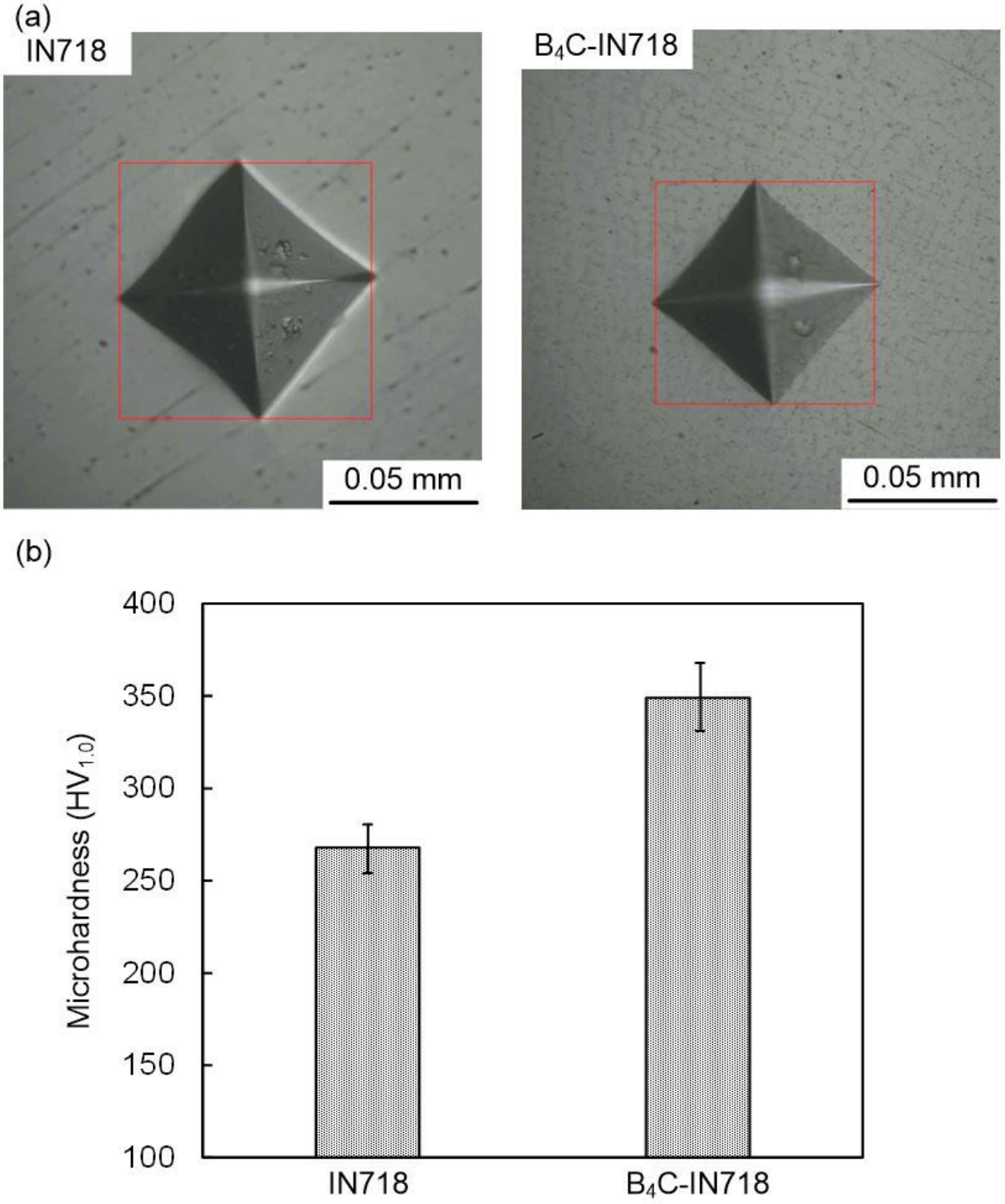

Figure 8

Microhardness of laser DED fabricated Inconel 718 coatings and B_4C-Inconel 718 coatings: (a) optical microscope image and (b) microhardness values

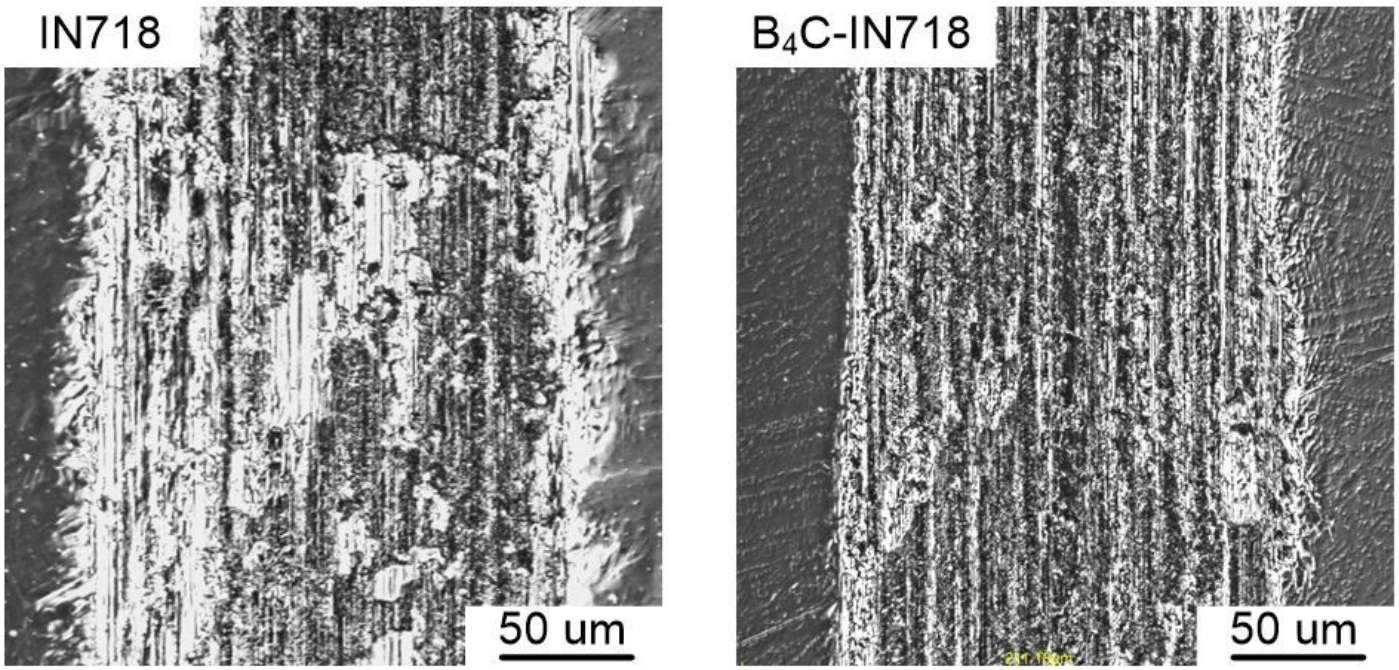

Figure 9

Worn surface morphologies of laser DED fabricated Inconel 718 coatings and B_4C-Inconel 718 coatings

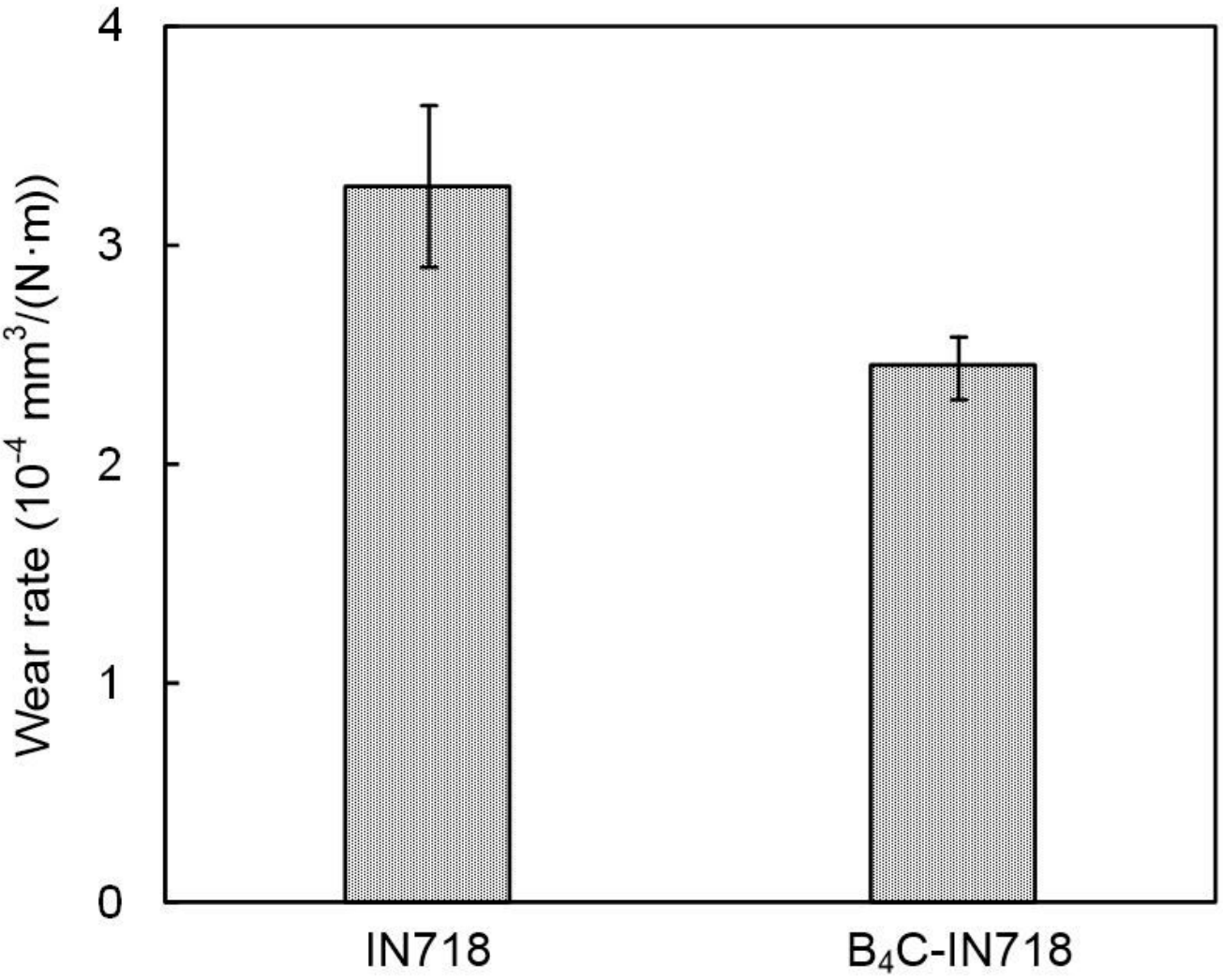

Figure 10

Wear resistance of laser DED fabricated Inconel 718 coatings and B_4C-Inconel 718 coatings